Adaptive Detection and ISI Mitigation for Mobile Molecular Communication

Ge Chang, Lin Lin, and Hao Yan*

Abstract

Current studies on modulation and detection schemes in molecular communication mainly focus on the scenarios with static transmitters and receivers. However, mobile molecular communication is needed in many envisioned applications, such as target tracking and drug delivery. Until now, investigations about mobile molecular communication have been limited. In this paper, a static transmitter and a mobile bacterium-based receiver performing random walk are considered. In this mobile scenario, the channel impulse response changes due to the dynamic change of the distance between the transmitter and the receiver. Detection schemes based on fixed distance fail in signal detection in such a scenario. Furthermore, the intersymbol interference (ISI) effect becomes more complex due to the dynamic character of the signal which makes the estimation and mitigation of the ISI even more difficult. In this paper, an adaptive ISI mitigation method and two adaptive detection schemes are proposed for this mobile scenario. In the proposed scheme, adaptive ISI mitigation, estimation of dynamic distance and the corresponding impulse response reconstruction are performed in each symbol interval. Based on the dynamic channel impulse response in each interval, two adaptive detection schemes, concentration-based adaptive threshold detection (CATD) and peak-time-based adaptive detection (PAD), are proposed for signal detection. Simulations demonstrate that, the ISI effect is significantly reduced and the adaptive detection schemes are reliable and robust for mobile molecular communication.

This work was supported by National Natural Science Foundation, China (61502295, 61405111), the Shanghai Sailing Program through STCSM (14YF1408700), the National Key Research and Development Program of China (2016YFF0200705), and Shanghai Engineering Research Center for Intelligent diagnosis and treatment instrument (15DZ2252000).

G. Chang and H. Yan are with the School of Electronic, Information and Electrical Engineering Shanghai Jiao Tong University, Shanghai, 200240, China and with the Shanghai Engineering Research Center for Intelligent diagnosis and treatment instrument, Shanghai 200240, China (e-mail: sjtucg@sjtu.edu.cn; yan_hao@sjtu.edu.cn). Asterisk indicates corresponding author.

L. Lin is with the College of Electronics and Information Engineering, Tongji University, Shanghai, 201804 China (e-mail: fxlinlin@tongji.edu.cn).

I. INTRODUCTION

Emerging nanotechnology promises the use of molecular communication (MC) in nanonetworks, by which biological nanomachines (bio-nanomachines) can communicate with each other by sending and receiving molecules [1]. Being highly efficient and low-cost [2], MC is prevalent in nature and human bodies, e.g., in cell-cell communication. With the help of nanotechnology, MC may facilitate a plethora of applications from nano-electromechanical systems (NEMS) to in-body health monitoring [3].

A nanomachine is the basic element in a MC system. Its size ranges from nanometers to micrometers. There are three different approaches for the development of nanomachines, including top-down approach, bottom up approach, and hybrid approach [1]. Genetically engineered cell, as a bottom up approach, is a good candidate for the development of bio-nanomachines. Among assorted cells that could be used as bio-nanomachines, flagellate bacteria are universally used in genetic engineering. For example, Escherichia coli (*E. coli*) is one kind of bacterium with flagella having the advantages including being low cost and easy to produce [4] and has been considered as the communicating nanomachines in MC [5].

MC for static nanomachines has been intensively studied in the past few years [6]–[10]. However, mobile MC has received little attention so far, although it can be envisioned as a potential scenario in many applications. For example, a group of nanorobots could communicate and coordinate with each other to move towards cancer cells to release drugs [11]. In [12], digital MC systems in blood vessels were established, where the transmitter nanomachine is mobile. A clock synchronization scheme was proposed for a similar mobile scenario in [13]. In [14] and [15], fluorescence resonance energy transfer (FRET) based mobile molecular nanonetworks was considered. The communication theoretical analysis as well as coverage and throughput analysis were conducted. Another kind of mobile ad hoc nanonetworks is proposed for collision-based MC [11]. A positional-distance codes scheme was proposed for mobile MCs and a hardware experiment based on a macro-scale testbed was performed [16]. The mobility pattern of nanoparticles, e.g., *E. coli*, was described in [17]. However, the investigations on signal detection schemes for mobile MC are rare. Only recently, a simple detection method for mobile MC was proposed in [18] without considering intersymbol interference (ISI) effect. Ref. [19] proposed a bit alignment technique for mobile scenario without providing details for detection. More in-depth investigations on signal detection schemes for mobile MC are needed.

In the mobile MC, two categories of problems arise. One problem is that the time-varying impulse response (IR) of the diffusion channel may influence the signal detection. When the transmitter releases molecules, the molecules move randomly based on the Brownian motion. According to the Fick's second law of diffusion, the expected IR of the diffusion channel is a function of time and the distance between the transmitter and the receiver. The concentration at the receiver increases quickly until reaching its maximum, and decreases slowly, forming a long tail [20]. If the transmitter and the receiver are static, the expected IR is only a function of time and is always the same. However, if the transmitter and/or the receiver is mobile, then the expected IR varies due to the random change of the distance between the transmitter and the receiver. For example, if the transmitter and the receiver get closer, the shape of the expected IR changes in that its peak amplitude increases while the peak time decreases. This fact impacts the signal detection at the receiver side if the detection scheme for the static MC is still used.

Another problem is the complicated ISI effect [21], [22]. The ISI is caused by the long-tail of the channel IR. The residual molecules in the long-tail part of former symbols interfere with the molecules of the current symbol, which may cause incorrect signal detection. In the mobile MC, the ISI effect becomes more complicated, because the number of residual molecules from former symbols varies due to the nanomachine's mobility character, apart from the effect of noises caused by Brownian motion. In such case, the ISI effect is hard to calculate and mitigate. Hence, current ISI mitigation methods and adaptive threshold approaches considering ISI for static MC, such as [22], do not work well for the mobile case.

In this paper, two adaptive signal detection schemes and an ISI mitigation method for mobile MC are proposed. In each symbol interval, the receiver adaptively estimates the ISI and adaptively calculates the threshold to make a decision. In contrast to the studies on signal detection for the static MC, this work deals with the issues caused by the mobile features. To the best of the authors' knowledge, approaches to mitigate the ISI effect and perform adaptive signal detection for the mobile MC has not been studied yet. The main contributions of this work lie in the following three parts:

1) A three-dimensional channel model for the mobile MC is established considering *E. coli*'s mobility nature.
2) An adaptive ISI mitigation method is proposed for mobile MC.
3) Two adaptive detection schemes are proposed for mobile MC.

The remainder of this paper is organized as follows. In Section II, the related work about

signal detection for MC is described. Section III presents the system model including the mobility model and the channel model for mobile scenario. Section IV discusses the two main problems associated with mobile MC. To solve the problem in mobile MC system, Section V proposes an adaptive ISI mitigation approach and two adaptive detection schemes. In Section VI, simulations are performed to evaluate the proposed schemes. The results show that the proposed ISI mitigation method can effectively suppress ISI effect and the adaptive detection schemes are effective in the signal detection for mobile MC scenario. Finally, Section VII concludes the paper.

II. Related Work

In this section, the related work on signal detection in MC is presented. Due to the MC channel property, the molecule concentration at the receiver side spreads. Signal detection refers to the process of extracting the original information from the received signal after the transformation through the channel. In addition, the channel noise, such as additive noise or ISI, corrupts the modulated signal, which makes the detection more difficult.

Different types of modulation techniques need different detectors. For MC, concentration-based modulation and type-based modulation are the two main widely used modulation techniques [23], [24]. Many works focus on the detection issues for either concentration-based modulation [9], [10], [21], [22], [25]–[29] or type-based modulation [30], [31], or concentration and type combined modulation scheme [32]. In this paper, we focus on the on-off keying (OOK) concentration-based modulation.

The basic process for signal detection includes two steps: 1) sampling the received signal and 2) comparing the sample with a threshold to make a decision. An important issue in the detection process is to remove the ISI effect. Increasing symbol interval may be one solution to mitigate the effect of ISI. However, this sacrifices the data rate, which is undesirable. The existing research works proposed different detection schemes balancing the probability of error and computational complexity for different data rates. These previous detection schemes, however, are proposed for the fixed transmitter and receiver, rather than mobile scenario. Some adaptive detection methods are proposed for better decoding performance considering the ISI effect. In [25], the authors proposed two detection schemes, namely, sampling-based detection and energy-based detection for OOK modulation techniques. The receiver samples the molecule concentration at a time or accumulates the molecule concentration for a bit period, and then compares the value with a

pre-defined threshold to make a judgement. In [27] and [28], theoretical formulations and architectures of the strength-based optimum receivers based on spike transmission of molecules were presented in the presence of both diffusion noise and ISI. The optimum and sub-optimum versions of amplitude-shift keying (ASK) and OOK receivers were designed. In [10], the authors proposed sequence detection methods based on maximum a posteriori (MAP) and maximum likelihood (ML) criterions. A linear equalizer based on minimum mean-square error (MMSE) criterion and a decision-feedback equalizer (DFE) were also proposed which reduce the probability of error detection. Similar ideas were proposed in [33], which accounts for the possibility of the presence of the steady uniform flow in any arbitrary direction, unwanted molecules from other source, and enzymes in the propagation environment to degrade the information molecules. In [22], an analytical technique is proposed to determine the optimum threshold. A new modulation called molecular transition shift keying (MTSK) was proposed to decrease the effects of ISI and enhance energy efficiency. A power adjustment technique that utilizes the residual molecules was proposed. A low-complexity non-coherent signal detector for nanoscale MCs was proposed which can suppress ISI effectively [21]. A detection algorithm for a molecular multiple-input multiple-output (MIMO) scenario is proposed in [34].

Current ISI mitigation and detection methods are based on the situation where the distance between the transmitter and the receiver is fixed. Because the distance in the whole communication does not change, the IR stays the same. If the former symbol values are known, the effect of ISI on the current symbol is predictable. However, in the scenario of the mobile MC, the distance between the transmitter and receiver changes all the time due to the random movement of the nanomachines. The corresponding IR at the receiver changes correspondingly. This means we cannot obtain a fixed optimal threshold to detect all the transmitted symbols. Therefore, the proposed detection schemes in the literature without considering the mobility of nanomachines will not work anymore for the mobile scenario. Furthermore, the existing ISI mitigation methods based on the fixed IR are also not valid in the mobile scenario. Even if the former symbols are correctly detected, the number of molecules expected at the receiver due to previous intervals randomly changes due to the randomness of the distance. Therefore, the existing detection proposals for the static MC scenario are no longer applicable for the mobile scenario.

In this paper, appropriate signal detection schemes along with an effective ISI mitigation method for mobile MC are proposed.

III. System Model

In an isotropic environment without fluid velocity, a MC system between a static transmitter and a mobile receiver performing random walk is considered. The transmitter is modeled as a fixed point. One kind of flagellated bacterium, *E. coli* with volume V_R, is adopted as the mobile receiver [17]. The receiver is a "passive" type receiver. It can sense the concentration within its observation volume. But such sensing behavior will not impede the diffusion of the molecules. This kind of passive type receiver has been widely used in many literature such as [35], [36].

In the first subsection, according to *E. coli*'s characteristics, the receiver's mobility is modeled. In the second subsection, a mobile three-dimensional channel model of MC is introduced by incorporating the receiver's mobility.

A. Mobility Model

As a well studied prokaryotic cell in biological engineering, *E. coli* has been frequently adopted as a mobile nanomachine in the MC studies [5], [37]. It has a group of flagella to decide its motion status, which falls into two categories, *run* mode and *tumble* mode with the flagella turning counterclockwise and clockwise, respectively [17]. These two modes alternate.

The mobility model of *E. coli* has been investigated in [5], [17], [37]. In this work, we refer to the model in [17] and [5]. In the *run* mode, *E. coli* executes a linear motion with a constant velocity V_r in a constant direction of θ. In the *tumble* mode, *E. coli* changes its moving direction. The *tumble* mode is much shorter than the *run* mode in practice. The Poisson distribution is adopted to describe the alternation between the two modes [17]. For each unit time, the occurrence of the *run* and *tumble* modes follows the Poisson distribution with parameters λ and 1-λ, respectively. We take the *run* mode as an example. The probability that *run* mode occurs between time t and $t + \Delta t$ is

$$P(t; \lambda)\Delta t = \lambda e^{-\lambda t}\Delta t. \tag{1}$$

(1) is the Poisson interval distribution (please refer to Eq 6.8 in [17]).

In three dimensional isotropic environment, for each tumble, the receiver would change its direction from θ_0 to $\theta = \theta_0 + \Delta\theta$ [5], [17]. The random variable $\Delta\theta$ equals to ϕ or $-\phi$ with equal probabilities. The mean and variance of θ at time $t + \Delta t$ are

$$E[\theta] = \theta_0, \tag{2}$$

$$\text{Var}[\theta] = 4D_r\Delta t, \tag{3}$$

where D_r is the rotational diffusion constant [17]. This can be obtained through the Einstein-Smoluchowski relation as

$$D_r = \frac{k_b T}{f_r}, \tag{4}$$

where k_b is the Boltzman constant, T is the absolute temperature in the environment, and f_r is the rotational frictional drag coefficient.

The three dimensional angle θ could be expressed as $\theta = (\theta_{xy}, \theta_z)$ with θ_{xy} be the azimuthal angle and θ_z be the polar angle. The location changes in each *run* step with the initial angle θ are

$$\begin{aligned} \Delta x &= V_r \Delta t \sin\theta_z \cos\theta_{xy}, \\ \Delta y &= V_r \Delta t \sin\theta_z \sin\theta_{xy}, \\ \Delta z &= V_r \Delta t \cos\theta_z. \end{aligned} \tag{5}$$

The fixed transmitter is located at (x_0, y_0, z_0) and the mobile receiver is initially located at $(0, 0, 0)$. If the dynamic location of the receiver in random walk is $[x'(t), y'(t), z'(t)]$, then the dynamic distance between the transmitter and receiver, $d(t)$, could be expressed as

$$d(t) = \sqrt{[x'(t) - x_0]^2 + [y'(t) - y_0]^2 + [z'(t) - z_0]^2}. \tag{6}$$

Based on the moving characteristics of *E. coli* discussed above, a sample trajectory of *E. coli*'s random walk in a three dimensional environment is shown in Fig 1. Cartesian coordinate is used to describe the location of the receiver. Note that the rotational diffusion coefficient varies in different environments and will largely determine the motion trail of the receiver [6] such as *E. coli*.

B. Mobile MC Model

The model of MC via diffusion is illustrated in Fig. 2. The model includes a transmitter nanomachine, molecule diffusion channel, additive and signal-dependent noise and a receiver nanomachine. The symbol sequence $\{a_j\}$ is modulated by the transmitter into the molecule concentration pulses $s(t)$ which is released by the transmitter into the diffusion channel with an impulse response $h(t)$. The information molecules then propagate in the aqueous medium via

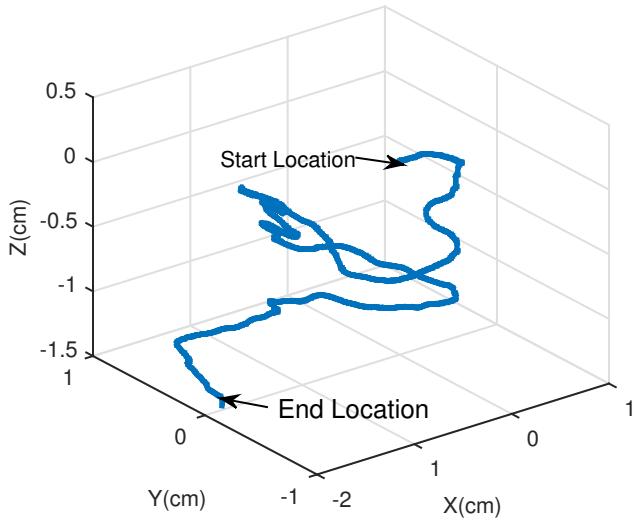

Fig. 1. An instance of the mobile receiver's motion trajectory. Based on the *E. coli*'s moving characteristics, the trail of the receiver is simulated with 500000 simulation steps with $\lambda = 0.9$. The initial position of the receiver is $(0, 0, 0)$ and it has a initial velocity V_r.

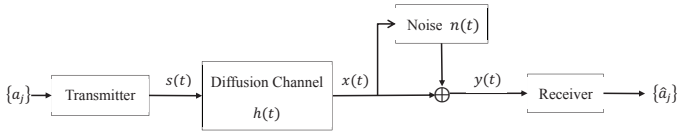

Fig. 2. The model of MC via diffusion.

diffusion. And part of the information molecules arrive at the receiver and its concentration is $x(t)$. At receiver, an additive and signal-dependent noise $n(t)$ exists. The receiver nanomachine senses the noisy molecule concentration $y(t) = x(t) + n(t)$ to detect the transmitted information sequence $\hat{\{a_j\}}$.

Firstly, we discuss the impulse response of the diffusion channel. In the diffusion channel, the information molecules propagate from the transmitter to the receiver according to the concentration gradient. According to the Fick's second law of diffusion [6], the concentration of molecules, denoted by $C(x', y', z', t)$, at a receiver location (x', y', z') and time t is described by

$$\frac{\partial C(x', y', z', , t)}{\partial t} = D\nabla^2 C(x', y', z', , t), \tag{7}$$

where ∇^2 and D are Laplacian operator and diffusion coefficient, respectively. The expected

channel IR for a fixed receiver is obtained by solving (7) with the initial condition

$$C(x', y', z', t = 0) = \delta(x' - x_0, y' - y_0, z' - z_0). \tag{8}$$

The solution of (7) with the initial condition in (8) is the expected IR of the diffusion channel for the static MC with a fixed distance $d = \sqrt{(x' - x_0)^2 + (y' - y_0)^2 + (z' - z_0)^2}$ which is expressed as [10]

$$h(t) = \frac{1}{(4\pi Dt)^{\frac{3}{2}}} \exp\left(-\frac{d^2}{4Dt}\right). \tag{9}$$

In the mobile scenario, the distance is not a constant, but in dynamic change as described by (6). By substituting d in (9) with the variable $d(t)$ in (6), the expected channel IR of the diffusion channel for the mobile MC is

$$h[d(t), t] = \frac{1}{(4\pi Dt)^{\frac{3}{2}}} \exp\left[-\frac{d^2(t)}{4Dt}\right]. \tag{10}$$

In the following part of this paper, we call the expected IR of the diffusion channel as IR for short.

In our mobile MC model, one symbol interval is divided into multiple steps to better resolve the distance change caused by the receiver's random walk. Hence, each step has a different distance and a corresponding IR according to (10). The channel IR in an interval becomes a composite of individual IR values as shown in Fig. 3 as an example. The points of the true IR in one interval are from different IR plots based on different physical distances due to the random nature of the receiver. Therefore, the true IR cannot be exactly expressed or fitted by one individual equation as in (9) with a constant d. However, a good estimate of the true IR by a reconstructed IR with a constant d is possible. This will be discussed in Section V.

From a higher perspective of multiple intervals, the complete IRs in different intervals are different too, due to the randomness of positions caused by the random walk as illustrated by Fig. 4. Fig. 4 (a) shows the IRs of a series of symbol "1" for static scenario with a fixed distance while Fig. 4 (b) shows the IRs for the mobile scenario with variable distances. The corresponding random distance values are shown in Fig. 4 (c). From Fig. 4, we can see when the distance is fixed, the IRs are the same as in (a). However, when the distance changes as in (c), the shape of the IR also changes.

In the mobile MC model, an OOK modulation technique is adopted. Sending a bit "1" is represented by sending a pulse of N molecules and sending a bit "0" is represented by sending

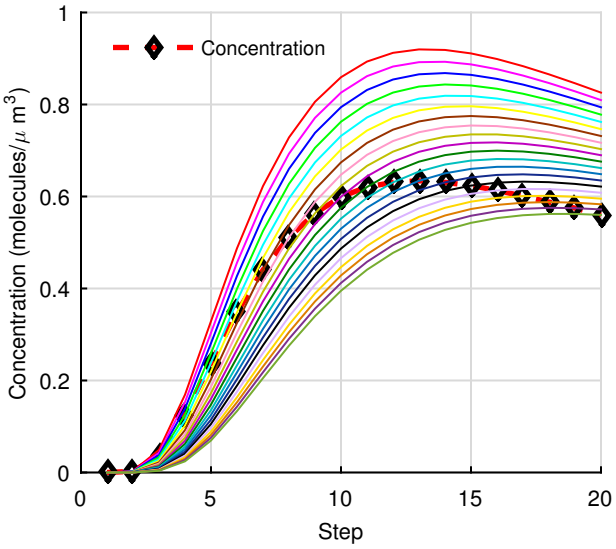

Fig. 3. An example of a complete true IR in one interval with multiple steps for a mobile scenario (Please refer to the color image in electronic pdf version to assist understanding). Different IR profiles determined by different distances at these steps with (9) are shown in different colors. The corresponding points of these IRs are highlighted by black diamond marks which forms the complete true IR in this interval. For this particular example, to present a more obvious illustration of the mobile scenario, the distance is set to keep increasing over the entire interval.

nothing [25]. We assume the duration of the pulse is much smaller than the symbol interval T_b such that $s(t)$ is

$$s(t) \approx \sum_{j=0}^{\infty} a_j N \delta(t - jT_b). \tag{11}$$

After propagation through the diffusion channel, the response of the channel to the input signal $s(t)$ is

$$x[d(t), t] = s(t) * h[d(t), t] = \sum_{j=0}^{\infty} a_j N h[d(t), t - jT_b] \tag{12}$$

where $*$ is the convolution operator. $x[d(t), t]$ is the noiseless molecule concentration signal at the receiver.

Basically, there are two types of noise sources, physical-sampling noise and physical-counting noise [38]. Since the physical sampling noise is negligible in the discrete binary concentration modulation [39], we only include counting noise in the study. The counting noise is the counting error at the receiver. It is generated due to the randomness of molecules in the movement and the

discreteness of the particles diffusion process [38]. The counting noise $n(t)$ can be considered as an additive signal dependent noise with zero mean [39] [40]:

$$n(t) \sim \mathcal{N}\left[0, \sigma_c^2(t)\right], \tag{13}$$

where $\sigma_c^2(t)$ is the variance, defined as

$$\sigma_c^2(t) = \frac{x[d(t), t]}{V_R}, \tag{14}$$

where $V_R = (4/3)\pi a^3$ is the volume of the spherical reception space of the receiver. Including the noise $n(t)$, the total noisy received concentration by the receiver $y[d(t), t]$ is

$$y[d(t), t] = \sum_{j=0}^{\infty} a_j N h[d(t), t - jT_b] + n(t). \tag{15}$$

Accordingly the total noisy received concentration by the receiver $y(t)$ for the static MC senario is

$$y(t) = \sum_{j=0}^{\infty} a_j N h(t - jT_b) + n(t). \tag{16}$$

Synchronization among nanomachines is assumed to be achieved. It is essential and especially pivotal for parameter estimation such as distance estimation. This assumption is widely used in literature such as [41], [42]. For the static MC scenario, there exist several synchronization protocols [43]–[45]. For the mobile scenario, the synchronization is actually more complicated. In [13], the authors proposed a method to estimate the clock offset based on the ML estimation in a mobile molecular communication system. We assume that this method can be conducted in our system to achieve the synchronization between nanomachines.

If the communication time is long enough, the receiver will move far away and the communication link will fail. Therefore, the definition of the lifetime of the communication is necessary. We define the lifetime in terms of distance. If the distance between the transmitter and the receiver reaches the lifetime distance d_{end}, we assume that the communication link is broken, which is beyond the scope of this paper. For initial distance d_0, the peak time is defined as $t_{0,\text{peak}}$. It is known that $t_{0,\text{peak}} = \frac{d_0^2}{6D}$ (this can be derived by the impulse response equation). It is assumed that the symbol interval is $T_b = m \times t_{0,\text{peak}}$, where m is a positive integer. We define the position that the peak time is equal to the symbol interval is the lifetime distance d_{end}. By derivation, we have $d_{\text{end}} = d_0\sqrt{m}$. Based on the above definition, within the system lifetime, the peak point of the expected IR is always within the symbol interval.

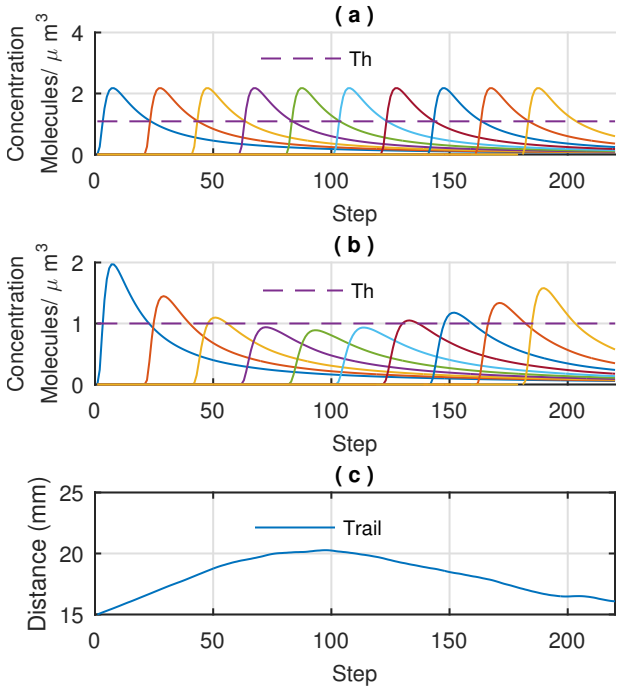

Fig. 4. Channel IRs in the static and mobile MC scenarios (Th denotes Thresholds). (a) Channel IRs in static MC scenario with the fixed distance of 15 mm. (b) Channel IRs in mobile MC scenario with the dynamic distance due to the random motion of the receiver. (c) The dynamic distances in the case of (b). Thresholds in (a) and (b) are defined as the half of the peak value of the IR of the initial distance. It is shown that, if ISI is appropriately mitigated, symbols could be correctly detected in static MC in (a) while some symbols could not be correctly detected in mobile MC in (b).

IV. Problem Statement

Due to the mobility of the receiver, the IR changes randomly. On one hand, this randomly varying IR complicates the signal detection compared to the static scenario. On the other hand, the ISI also varies due to the movement of the receiver, which makes the signal detection more challenging.

Firstly, the mobility impacts the signal detection. As shown in Fig. 4 (b), a predetermined fixed threshold fails in signal detection because of the dynamically changing amplitude of IR due to the mobility. For example, in the situation that the distance increases shown in the first half in Fig. 4(c), the amplitude of IR decreases. When it decreases to the value smaller than the threshold, symbol “1” is misdetected as “0”.

Secondly, the mobility complicates the ISI effect. The ISI effect is caused by the long tail of

the IR. The residual molecules of previous symbols interfere with the molecules of the current symbol. Since the receiver cannot distinguish molecules of the current symbol from the residual molecules of previous symbols, the signal detection is affected. In the mobile MC, ISI effect becomes more complicated because the IR is varying, meaning that the computation of the ISI in different symbol intervals uses different IRs. In the static nanomachine scenario, the receiver samples $y(t)$ of (16). We assume that the sampling rate $R = N_s/T_b$ with $N_s \in \mathbb{Z}^+$ which means we take N_s samples in each symbol interval T_b with a sampling interval of $T_s = T_b/N_s$. The sampled signal is expressed as

$$y_k = N \sum_{j=0}^{\infty} a_j h_{k-jN_s} + n_k, \tag{17}$$

where $y_k = y(kT_s)$, $h_{k-jN_s} = h(kT_s - jT_b) = h(kT_s - jN_sT_s)$, and $n_k = n(kT_s)$ with the sampling index $k = 0, 1, ..., \infty$. For $k - jN_s < 0$, we will have $h_{k-jN_s} = 0$. Then (17) can be further simplified as

$$y_k = N \sum_{j=0}^{\lfloor k/N_s \rfloor} a_j h_{k-jN_s} + n_k, \tag{18}$$

where $\lfloor\ \rfloor$ represents the floor function. If we further distinguish the molecule concentration of the current symbol from the ISI signal of former symbols, (18) can be expressed as

$$y_k = N a_{\lfloor k/N_s \rfloor} h_{k-\lfloor k/N_s \rfloor N_s} + N \sum_{j=0}^{\lfloor k/N_s \rfloor - 1} a_j h_{k-jN_s} + n_k, \tag{19}$$

where $N a_{\lfloor k/N_s \rfloor} h_{k-\lfloor k/N_s \rfloor N_s}$ is the molecule concentration of the current symbol. $N \sum_{j=0}^{\lfloor k/N_s \rfloor - 1} a_j h_{k-jN_s}$ is the ISI signal from former symbols. If we further define

$$y_{\text{current},k} = N a_{\lfloor k/N_s \rfloor} h_{k-\lfloor k/N_s \rfloor N_s}, \tag{20}$$

and

$$y_{\text{ISI},k} = N \sum_{j=0}^{\lfloor k/N_s \rfloor - 1} a_j h_{k-jN_s}, \tag{21}$$

the received signal in (18) can be expressed as

$$y_k = y_{\text{current},k} + y_{\text{ISI},k} + n_k. \tag{22}$$

The receiver cannot distinguish $y_{\text{current},k}$ from y_k, which causes incorrect signal detection. This phenomenon with a fixed distance is illustrated in Fig. 5. The transmitted symbol sequence is [1100100]. The dash-dot blue, green and red curves are the individual IRs for each symbol. The

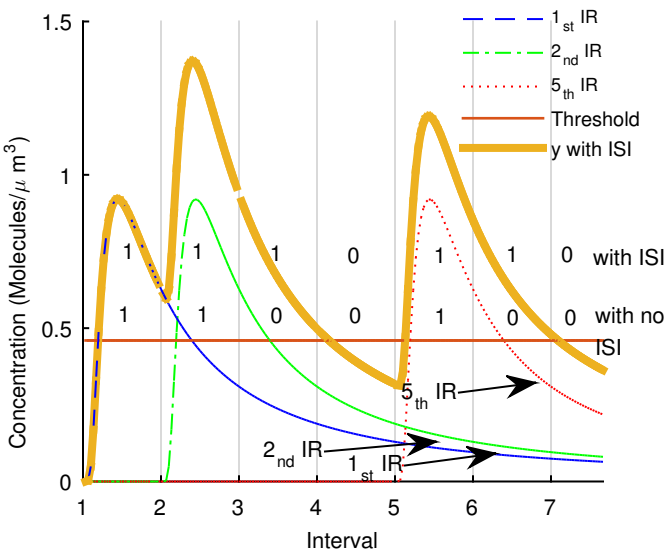

Fig. 5. Illustration of the ISI effect in static MC. The distance between the transmitter and the receiver is fixed. Diffusion coefficient is 5 rad^2/s. The transmitted symbol sequence is [1 1 0 0 1 0 0]. The dash-dot blue, green and red curves are the individual IRs for each symbol. The solid dark yellow curve is the total received concentration including the ISI effect. The threshold is set as the half of the peak concentration value. Due to the ISI effect, the detection result is [1 1 1 0 1 1 0]. Note that the noise term is not reflected in this figure.

solid dark yellow curve is the total received concentration including the ISI effect. The noise is not included since we would like to highlight the effect of the ISI. The 3th and 6th symbols are incorrectly detected as "1" due to the ISI effect.

In the mobile scenario, mobility complicates the ISI effect. The IR is not only the function of time, but also the function of a random distance as discussed in (10). In the discrete form, the random distance $d(t)$ and the corresponding discrete form of IR of (10) become $d_k = d(kT_s)$, and $h_{d_k,k-jN_s} = h[d(kT_s), kT_s - jN_sT_s]$. Therefore, in mobile MC, the received sampled signal $y_{d_k,k}$ become

$$y_{d_k,k} = Na_{\lfloor k/N_s \rfloor} h_{d_k,k-\lfloor k/N_s \rfloor N_s} + N \sum_{j=0}^{\lfloor k/N_s \rfloor - 1} a_j h_{d_k,k-jN_s} + n_k. \tag{23}$$

It could be further expressed as

$$y_{d_k,k} = y_{\text{current},d_k,k} + y_{\text{ISI},d_k,k} + n_k, \tag{24}$$

where $y_{\text{current},d_k,k}$ and $y_{\text{ISI},d_k,k}$ are

$$y_{\text{current},d_k,k} = Na_{\lfloor k/N_s \rfloor} h_{d_k,k-\lfloor k/N_s \rfloor N_s}, \tag{25}$$

and

$$y_{\text{ISI},d_k,k} = N \sum_{j=0}^{\lfloor k/N_s \rfloor - 1} a_j h_{d_k,k-jN_s}. \tag{26}$$

$h_{k-\lfloor k/N_s \rfloor N_s}$ in (20) and h_{k-jN_s} in (21) becoming $h_{d_k,k-\lfloor k/N_s \rfloor N_s}$ in (25) and $h_{d_k,k-jN_s}$ in (26) makes the mobile scenario more complicated. Fig. 6 illustrates the ISI effect in a mobile MC. One symbol "1" is transmitted by sending N molecules. We discuss its ISI effects on the following three intervals at the receiver. Due to the mobility, each interval has a different distance and a corresponding IR presented by the green, pink, yellow, and red curves. The ISI signals of the symbol on the 2nd, 3rd and 4th intervals are black circles on the pink, yellow, and red curves. Therefore, it can be seen that in mobile MC the ISI changes due to the change of distance. We should note that Fig. 6 only illustrates the ISI from one transmitted symbol "1". However, the ISI is the accumulated interference from all former symbols. This makes the signal degradation in the mobile scenario more complicated. Hence investigation of detection schemes suitable for the mobile MC is quite necessary.

V. Proposed Detection Scheme

In this section, we propose a detection scheme for the mobile MC with a mobile receiver. The aim of the proposed scheme is to overcome the problem caused by the mobility and complicated ISI in mobile MC to provide a solution for correct detection in mobile MC.

A. Overall Scheme

The proposed scheme includes an adaptive ISI mitigation method, distance estimation and IR reconstruction, and two adaptive signal detection methods as illustrated in Fig. 7. Firstly, samples are taken by the receiver. Next, the receiver checks whether there was symbol "1" released in the former detected symbol sequence. If no symbol "1" has been detected, we use the samples to directly estimate the distance for the current symbol. Based on the estimated distance, the IR for the current interval is reconstructed and its peak concentration and peak time are obtained. Then two adaptive detection methods, concentration-based adaptive threshold detection (CATD) and peak-time-based adaptive detection (PAD) methods, are adopted to detect the current symbol. The detection result and the estimated distance are stored for the ISI calculation of the following symbols.

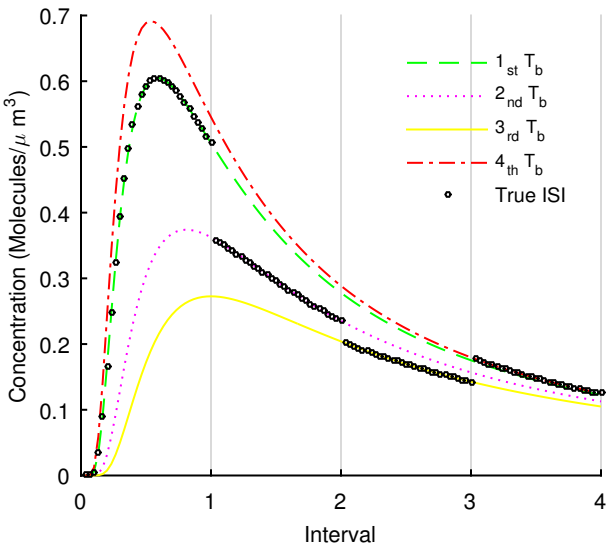

Fig. 6. Illustration of the ISI effect in a mobile MC. The transmitter sends a symbol "1". The ISI effect of this single symbol on the following intervals are considered in this example. The dashed green, dotted pink, solid yellow, and dash-dotted red curves are the IRs at the receiver with different distances in the 1st, 2nd, 3rd, and 4th interval which are 27 mm, 30 mm, 33 mm, 23 mm, respectively. The black circles on the green, pink, yellow, and red curves are the real concentrations of the symbol in the four intervals. The ISI signals are the highlighted black circles in the last three intervals. We should note that, to simplify the illustration, each interval is assigned with a fixed distance which is not the model used for the rest of the work where each step is assigned with a random distance.

If there is symbol "1" detected previously, ISI mitigation is implemented before distance estimation step. The reason is to reduce the influence of the ISI effect on current symbol and improve the detection accuracy. With ISI effect, the signal of current symbol could be distorted. The distortion is severe especially at high data rate in mobile MC where ISI effect is severe and random. With the severely distorted samples, the distance estimation and the IR reconstruction cannot be accurate. This eventually affects the signal detection and causes high bit error rate (BER) or even failure in detection. Therefore, for accurate detection, ISI mitigation is implemented before other processes. To accomplish such ISI mitigation, the distance estimated from former symbol intervals, instead of the distance in the current symbol interval, is utilized in the ISI calculation. Then the ISI mitigated data are used in the following procedures including distance estimation, IR reconstruction, and adaptive signal detection as discussed above.

As discussed in Section IV, the core of the two problems lies in the dynamic distance in mobile MC. Therefore, the main idea of our solution is to dynamically estimate the varying

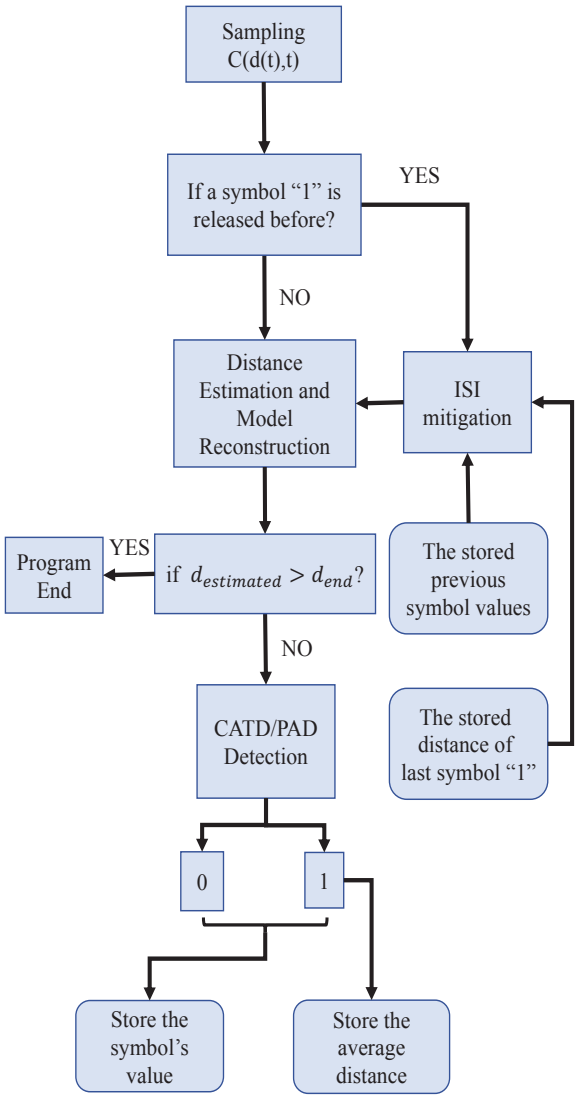

Fig. 7. The proposed detection scheme in one interval.

distance, from which we calculate the adaptive threshold to compare with the sampled signal to make decision.

The functional blocks including distance estimation and IR reconstruction, CATD/PAD detection, and adaptive ISI mitigation are discussed in the following subsections in detail.

B. Detailed Scheme

1) Distance Estimation and IR Reconstruction: An important step in the proposed scheme is to estimate the dynamic distance with the samples and use the dynamic distance to reconstruct

the corresponding dynamic IR in one interval. Here the samples and data used are referred to as the ISI reduced samples and data as

$$\begin{aligned} z_{d_k,k} &= y_{d_k,k} - \hat{y}_{\text{ISI},d_k,k} \\ &= y_{\text{current},d_k,k} + y_{\text{ISI},d_k,k} - \hat{y}_{\text{ISI},d_k,k} + n_k, \end{aligned} \tag{27}$$

where $\hat{y}_{\text{ISI},d_k,k}$ is the estimated ISI signal. The ISI mitigation will be discussed in detail in Section V-B-3. If the estimation is good enough, the ISI reduced signal $z_{d_k,k}$ can be expressed as

$$z_{d_k,k} = y_{\text{current},d_k,k} + n_k. \tag{28}$$

To focus on the analysis and evaluation of the mobility feature, it is assumed that the signal-to-noise ratio (SNR) is sufficiently large meaning that the noise is small. Then we have

$$z_{d_k,k} \approx y_{\text{current},d_k,k}. \tag{29}$$

If the SNR is not large enough, (29) can also be obtained if a MIMO system is used for spatial diversity [46].

$z_{d_k,k}$ in (29) is used to estimate the distance. Methods of the parameter estimation, especially the distance estimation, have been proposed in the literature. In [47], round-trip-time protocol based on single spike feedback signals was proposed to measure the distance. One nanomachine releases a single spike of type A molecules. Once the other nanomachine detects A molecules, it releases a single spike of type B molecules immediately. The original nanomachine detects the type B molecule. Then the round-trip-time is used to measure the distance. In [48], the authors derived the ML distance estimator by maximizing the joint observation likelihood function. In [49], one symbol transmission is adopted. The peak concentration value is used to estimate the distance. In [50], a similar idea was proposed but the distance is calculated by the peak concentration time in one symbol transmission. In our scheme, a method close to [49] is used to estimate distance.

In the case symbol "1" is transmitted such that $a_{j=\lfloor k/N_s \rfloor} = 1$, based on (10) and (25), the distance d_k can be computed with each sample $z_{d_k,k}$ as

$$\begin{gathered} d_k = \left| 2(-DkT_s \ln \frac{z_{d_k,k}(4\pi DkT_s)^{\frac{3}{2}}}{N})^{\frac{1}{2}} \right|, \\ k \in \mathbb{Z}^+ \text{ and } jN_s \leq k < (j+1)N_s. \end{gathered} \tag{30}$$

Due to random walk of the receiver, the true distances in each interval are not the same for different samples. Hence an averaged distance is calculated for that interval. The averaged distance in the jth symbol interval, $d_{j,\text{ave}}$, can be expressed as

$$d_{j,\text{ave}} = \frac{\sum_{k=jN_s}^{(j+1)N_s-1} d_k}{N_s}. \tag{31}$$

With $d_{j,\text{ave}}$, the IR in the jth interval $h(d_{j,\text{ave}}, t)$ can be computed by (10):

$$h(d_{j,\text{ave}}, t) = \frac{1}{(4\pi Dt)^{\frac{3}{2}}} \exp\left(-\frac{d_{j,\text{ave}}^2}{4Dt}\right). \tag{32}$$

Its peak time $t_{j,\text{peak}}$ could be calculated by setting the derivative of (32) to zero and be expressed as

$$t_{j,\text{peak}} = \frac{d_{j,\text{ave}}^2}{6D}. \tag{33}$$

The peak value of (32), $h_{j,\text{peak}}$, is

$$\begin{aligned} h_{j,\text{peak}} &= h(d_{j,\text{ave}}, t_{j,\text{peak}}) \\ &= \frac{1}{\left(\frac{2\pi}{3}\right)^{\frac{3}{2}} d_{j,\text{ave}}^3} \exp^{-\frac{3}{2}}. \end{aligned} \tag{34}$$

If $d_{j,\text{ave}}$ is a good estimate of the distance range in an interval, $h(d_{j,\text{ave}}, t)$ is a good estimate of the true IR in that interval. The estimation accuracy analysis is given in Section V-C.

The calculated $d_{j,\text{ave}}$ and $h(d_{j,\text{ave}}, t)$ are good estimates for the case of $a_j = 1$. In case of $a_j = 0$, the estimated distance and the reconstructed IR are incorrect. However, such correctness and incorrectness can be used for signal detection. Such signal detection methods are presented in detail in the next part.

2) Adaptive Signal Detection: In this work, two adaptive detection methods for the mobile MC are proposed.

In the static MC, signal detection is usually performed by comparing the amplitude of samples with a fixed threshold. In the mobile MC, the motion of the nanomachine leads to time-variant channel IR. Fixed threshold is no longer applicable. Therefore adaptive signal detection methods for mobile MC are proposed here. In Section V-B-1, the dynamic distance and dynamic IR are estimated in each interval. Based on the estimated dynamic IR, adaptive signal detections are implemented in each interval.

As mentioned in Section V-B-1, the samples are used to reconstruct the IR assuming symbol "1" is transmitted. Therefore, the characteristics of the reconstructed IR are different in the

cases that the symbol "1" or "0" is transmitted. Fig. 8 illustrates these characteristics of the reconstructed IR. Two situations of symbol value "0" and "1" with the same system parameters are shown in the left and right panes, respectively. In both cases, the received signal in an interval is the blue curve. The arrows (left) and diamonds (right) are taken samples. Based on the samples, IRs are reconstructed as shown by the dotted red (left) and dash-dotted red (right) curves in the two panes. By comparing the two reconstructed IRs in the two figures, it is seen that the reconstructed IR for symbol "1" fits the samples well while the reconstructed IR for symbol "0" does not. In the case for symbol "0" transmitted, the concrete differences of the reconstructed IR from received samples are present in both the amplitude and time. Firstly, the amplitude of the samples are much smaller than the peak amplitude of the reconstructed IR. Secondly, the peak time of the reconstructed IR falls outside of the symbol interval, which will not happen within the system lifetime. Furthermore, the two reconstructed IRs for symbol "0" and "1" are different, though with the same system parameter. The reconstructed IR for symbol "1" approximates the true IR well. But the reconstructed IR for symbol "0" is not correct. Its amplitude is much smaller than the true IR and its peak time is much larger than the true IR.

Based on the above characteristics, we propose two adaptive detection methods, the CATD method and PAD method.

In CATD scheme, before a symbol "1" is detected, the signal detection is implemented by comparing sample values $\{z_{d_k}\}$ with half of the peak amplitude of the reconstructed IR in current interval with the following criterion:

$$\hat{a_j} = \begin{cases} 1, & \max\left(z_{d_k}\right) \geq \frac{1}{2} h_{j,\text{peak}}, \\ & k \in \mathbb{Z}^+ \text{ and } jN_s \leq k < (j+1)N_s, \\ 0, & \text{otherwise.} \end{cases} \tag{35}$$

After a symbol "1" is detected, the signal detection is implemented by comparing the peak amplitude of the reconstructed IR in current jth interval $h_{j,\text{peak}}$ with half of the peak amplitude of reconstructed IR in last symbol "1" with the following criterion:

$$\hat{a_j} = \begin{cases} 1, & h_{j,\text{peak}} \geq \frac{1}{2} h_{*,\text{peak}}, \\ & k \in \mathbb{Z}^+ \text{ and } jN_s \leq k < (j+1)N_s, \\ 0, & \text{otherwise.} \end{cases} \tag{36}$$

where $*$ denotes the index of last symbol "1".

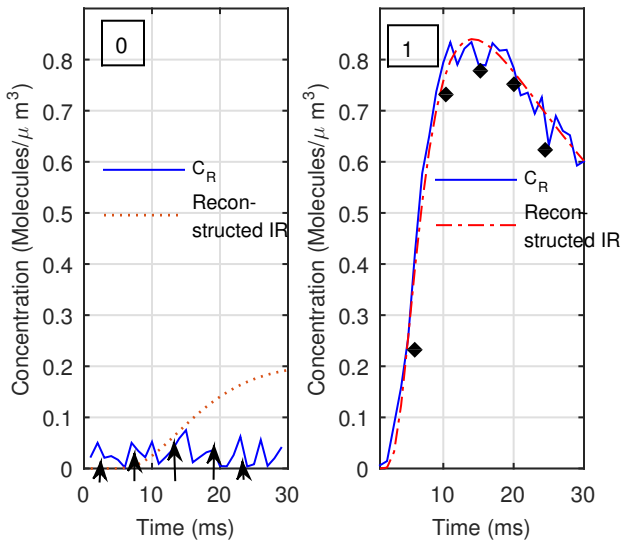

Fig. 8. IR reconstructions for symbol "0" (left figure) and "1"(right figure). Blue curves are the received signal for symbol "0" and "1". Arrows and diamonds highlight the sample points. Red dotted and red dash-dotted curves are the corresponding reconstructed IRs for symbol "0" and "1", respectively.

In PAD scheme, before a symbol "1" is detected, signal detection is implemented by comparing the peak time $t_{j,\text{peak}}$ of the reconstructed IR with the symbol interval T_b with the following criterion:

$$\hat{a_j} = \begin{cases} 1, & t_{j,\text{peak}} \leq T_b, \\ 0, & t_{j,\text{peak}} > T_b. \end{cases} \tag{37}$$

After a symbol "1" is detected, the signal detection is implemented by comparing the peak time $t_{j,\text{peak}}$ of the reconstructed IR in current jth interval with the peak time of reconstructed IR in last symbol "1" with the following criterion:

$$\hat{a_j} = \begin{cases} 1, & t_{j,\text{peak}} \leq 1.6 \times t_{*,\text{peak}}, \\ 0, & t_{j,\text{peak}} > 1.6 \times t_{*,\text{peak}}. \end{cases} \tag{38}$$

where the value 1.6 is choosen because that $h(d_{*,\text{ave}}, 1.6 \times t_{*,\text{peak}}) \approx \frac{1}{2} h(d_{*,\text{ave}}, t_{*,\text{peak}})$.

3) ISI Mitigation: ISI is the interference of former symbols on the current symbol. In OOK modulation, once a symbol "1" is released, ISI exists in the following symbol intervals. ISI mitigation is implemented to mitigate its impact on the following symbols and to improve the accuracy of the whole detection scheme.

To implement ISI mitigation, the key issue is the calculation of the ISI in the current interval. To calculate the ISI, the values of former symbols and the channel IR in the current interval should be known. However, the IR randomly changes and is difficult to obtain in mobile MC. This is because the position of the receiver changes all the time. Only if the distance between the transmitter and receiver is known, the IR in the current interval can be calculated. But, in our scheme, ISI mitigation is performed before the distance estimation. Therefore, the distance in the current interval and the corresponding IR is unknown when the ISI calculation is implemented.

To solve this problem, in the ISI calculation, we utilize the distance of the last symbol "1", $d_{*,\text{ave}}$ with $* \in \mathbb{Z}^+$and $* < j$, to approximate the distances d_k with $k \in \mathbb{Z}^+$ and $jN_s \leq k < (j+1)N_s$ for all the N_s samples in the current jth interval. It should be noted that $d_{*,\text{ave}}$ is only adopted in the ISI calculation and mitigation. It will not be used in the distance estimation, IR reconstruction, and signal detection processes. The corresponding estimated ISI signal $\hat{y}_{\text{ISI},k}$ is

$$\hat{y}_{\text{ISI},d_k,k} = N \sum_{j=0}^{\lfloor k/N_s \rfloor - 1} a_j h_{d_{*,ave},k-jN_s}. \tag{39}$$

However, due to the difference between the true distance d_k and the approximated distance $d_{*,\text{ave}}$, an error exists between the true ISI $y_{\text{ISI},k}$ and the estimated ISI $\hat{y}_{\text{ISI},k}$ as

$$e_{\text{ISI}} = \hat{y}_{\text{ISI},d_k,k} - y_{\text{ISI},d_k,k}. \tag{40}$$

The error is due to the distance difference between $d_{*,\text{ave}}$ and the true distance, which could be further divided into two parts. One is caused by the difference between $d_{*,\text{ave}}$ in the $*$th interval and $d_{j,\text{ave}}$ in the jth interval. This error increases if the time duration $(j-*)T_b$ between $*$th and jth intervals gets larger. The other part is caused by the difference between the averaged distance $d_{j,\text{ave}}$ in the jth interval and the true distances $\{d_k\}$ with $k \in \mathbb{Z}^+$ and $jN_s \leq k < (j+1)N_s$ in the jth interval. This second part of error will be discussed in Section V-C.

4) An Example of the Entire Proposed Scheme: An example is provided in Fig. 9 to illustrate how the entire proposed detection scheme works. The transmitted symbol sequence is [1 1 0] with OOK modulation. With ISI, the true signal $y(t)$ at the receiver is shown in Fig. 9 (a) by the blue curve. The proposed detection scheme is applied as follows. The receiver takes samples of $y(t)$. In Fig. 9(b), samples $\{y_k\}$ in the first interval are not affected by ISI. Therefore no ISI mitigation is implemented in this interval. The samples $\{y_k\}$ are directly used to estimate the distance and reconstruct the IR with the estimated distance $d_{0,\text{ave}}$ shown by the yellow curve with

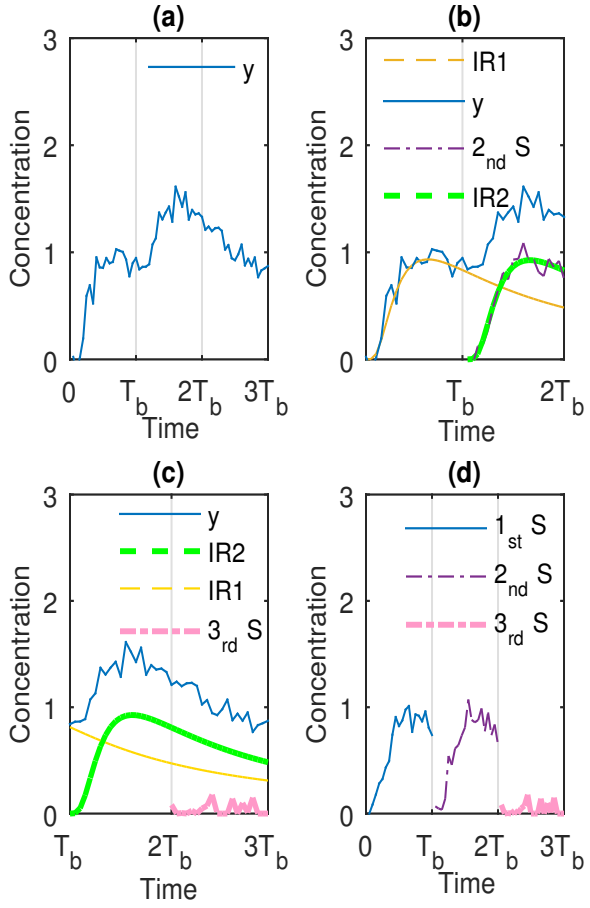

Fig. 9. Illustration of the proposed detection scheme. The unit of concentration in (a) to (d) is molecules/μm^3. The character "S" represents ISI mitigated signal. Symbol sequence [1 1 0] is transmitted with OOK modulation and is detected by the mobile receiver. (a) The received concentration at the receiver affected by both ISI effect and counting noise; (b) the signal detection process in the 1st and 2nd intervals. The yellow, purple and green curves are the reconstructed IR in the 1st interval, the ISI mitigated signal in the 2nd interval and the reconstructed IR in the 2nd interval, respectively; (c) the proposed detection in the 3rd interval. The yellow, green and pink curves are used to illustrate the ISI from the 1st symbol, the ISI from the 2nd symbol, and the ISI mitigated signal in the 3rd interval, respectively; (d) all the ISI mitigated signals in the three intervals which are further used for signal detection.

legend IR1 in (b). By comparing the curve IR1 with the samples taken in the 1st interval on the blue curves in (b), the proposed adaptive signal detection method (CATD or PAD) decodes the symbol as "1" and records the estimated distance value $d_{0,\text{ave}}$.

In the 2nd interval, the ISI is first calculated and mitigated. At this moment, the distance in the current interval is unknown. Because the last symbol is "1", the distance $d_{0,\text{ave}}$ recorded in the 1st interval is used as the approximated distance $d_{*,\text{ave}}$ for ISI calculation by (39). Then the calculated

ISI is mitigated from the received $y(t)$ (blue curve) in the 2nd interval. The ISI mitigated signal is shown by the purple curve with legend "2nd S" in (b). Note that when the ISI mitigated sample values are negative, they are set to zero in the calculation. Then distance estimation and IR reconstruction are performed based on these ISI mitigated samples. The reconstructed IR in the 2nd interval, IR2, is shown by the green curve in (b). The two adaptive detection methods decode the symbol as "1" by comparing the peak amplitude and time of the green curve IR2 with the peak amplitude and time of the reconstructed IR of last symbol "1" which is the yellow curve IR1 in the 2nd interval.

The process in the 3rd interval is similar to that in the 2nd interval. The only difference is that, both former symbols are included in the ISI calculation. The ISI mitigated signal is the "3rd S" denoted by the pink curve in (c). The proposed detection methods decode it as "0". Fig. 9(d) presents the ISI mitigated signals in all the three intervals. Comparing (d) with with (a), we can see that the ISI mitigation method is effective.

C. Accuracy Analysis and Parameter Design

In the mobile case, the distance randomly changes which makes the analytical derivation of the error probability very difficult. On one hand, the distance of the last symbol "1", $d_{*,\text{ave}}$, is used to approximate the current distance in ISI calculation, which introduces error. Due to the randomness, this error cannot be expressed mathematically in a closed-form expression. On the other hand, the threshold $h_{j,\text{threshold}}$, $t_{j,\text{peak}}$ and $h_{*,\text{threshold}}$, $t_{*,\text{peak}}$ are also dependent on the random distance. Therefore, it is very difficult to obtain the analytical expression of the error probability.

The accuracy of the proposed detection scheme including the ISI mitigation relies on the accuracy of the distance estimation and the corresponding reconstructed IR. As discussed in Section III, the reconstructed IR $h(d_{j,\text{ave}}, t)$ with a constant distance $d_{j,\text{ave}}$ in (31), at most, could be a good estimate of IR, but cannot be exactly the same as the true IR. Because the true IR is a composite of the points from different IRs, as shown in Fig. 3, it cannot be expressed by an IR with a constant distance. The aim of this subsection is to discuss the estimation accuracy of $h(d_{j,\text{ave}}, t)$ and how to design system parameters for accurate estimation.

For quantitative evaluation, correlation coefficient ρ is used to quantify the similarity of the reconstructed IR $h(d_{j,\text{ave}}, t)$ and true IR $h(d_k, t)$ with $k \in \mathbb{Z}^+$, $jN_s \leq k < (j+1)N_s$ as

$$\rho = \frac{\text{Cov}[h(d_{j,\text{ave}}, t)), h(d_k, t)]}{\sqrt{\text{Var}(h(d_{j,\text{ave}}, t))}\sqrt{\text{Var}(h(d_k, t))}}, \\ k \in \mathbb{Z}^+ \text{ and } jN_s \leq k < (j+1)N_s, \tag{41}$$

where $\text{Cov}(X, Y)$ is the covariance function of two variables X and Y, and Var is the data's variance. Larger ρ indicates a larger similarity and therefore a better estimate.

To achieve a good estimate of $h(d_{j,\text{ave}}, t)$, the average distance $d_{j,\text{ave}}$ should be a good estimate of $\{d_k\}$ with $k \in \mathbb{Z}^+$ and $jN_s \leq k < (j+1)N_s$ which is the range of random walk within one interval. For such purpose, the range of relative distance change in one interval should not be too large. We adopt relative distance change index r to define the maximum relative distance change in one interval as

$$r = \frac{d_{\text{max}}}{d_0} = \frac{V_r \times T_b}{d_0}, \tag{42}$$

where d_0 is the initial distance. d_{max} is the maximum possible distance change a receiver could reach in an interval. A larger r relates to a larger deviation in $d_{j,\text{ave}}$ from $\{d_k\}$ in one interval.

Next we investigate the relation of such deviation on the impact of the accuracy of the IR estimation. Simulations with different values of r are performed. With a value of r, a trajectory of random walk is generated. The distances are estimated and the IRs are reconstructed. The similarities between the reconstructed IR and the true IR are calculated by index ρ. The results are shown in Fig. 10 (results with $r = 5\%, 30\%$, and 50%) and Table I (more complete results with $r = 0.5\%, 5\%, 15\%, 30\%$, and 50%). The true IR and the reconstructed IR fit well with each other with $r = 0.5\%$. However their difference gets larger when r increases. Table I quantitatively shows that the similarity indicator ρ decreases when r increases which agrees with the result shown in Fig. 10. With r less than 5%, the correlation coefficient ρ between the estimated IR and the true IR is larger than 0.9988 which indicates that the established IR is a good estimate of the true IR. In this work, we define the situation with $r \leq 5\%$ as good conditions for estimation according to our investigation data.

Therefore, in order to achieve accurate IR reconstruction, system parameters including initial distance d_0, receiver velocity V_r, and interval length T_b should be selected to make the index r less than 5%.

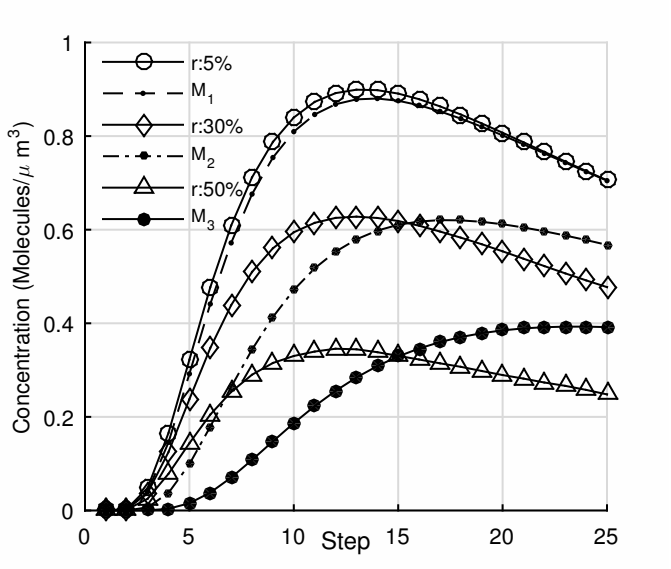

Fig. 10. IR reconstruction with different values of r. The value of r is selected from 5%, 30%, and 50%. The curves with legend r:5%, r:30%, r:50% are the true IRs with r equal to 5%, 30%, and 50%, respectively. The corresponding reconstructed IRs with our proposed methods are presented by curves with legend M_1, M_2 and M_3, respectively. The difference between the true and reconstructed IRs becomes larger with larger r.

TABLE I
CORRELATION COEFFICIENTS FOR INDEX VALUES

r	0.5%	5%	15%	30%	50%
Correlation Coefficient ρ	1	0.9988	0.9827	0.8687	0.5631

VI. SIMULATION RESULTS

In this section, the proposed detection scheme is evaluated by Monte Carlo simulations. Important system factors are investigated. These factors include the symbol sequence length, the symbol interval, the initial distance, and number of released molecules.

A. Simulation Parameters

In the simulations, a flagellated bacterium performing random walk is considered as the mobile receiver [51]. We assume that there is no drift velocity in the environment. The released molecules by the transmitter undergo the Brownian motion [24]. Unless otherwise stated, parameters in

TABLE II

SIMULATION PARAMETERS

Parameters	Symbol	Values
Symbol sequence length	B	7×10^4
Absolute temperature	T	305 K
Diffusion coefficient of information molecules	D	10^{-9} m^2/s
Number of molecules	N	3×10^6
Initial distance	d_0	$12\,\mu$m
Volume of spherical reception space of receiver	V_R	$1\,\mu$m^3
Symbol interval	T_b	96 ms
Peak time of channel IR at initial distance	$t_{0,\text{peak}}$	24 ms
Simulation step length	T_s	6 ms
Occurrence parameter of run modes	λ	0.9
Velocity of the receiver	V_r	$1.33\,\mu$m/s
Rotational diffusion coefficient of receiver	D_r	5 rad^2/s

Table II are adopted as default parameters in simulation based on [5], [17]. OOK is adopted as the modulation scheme.

An adaptive threshold detection (ATD) method is implemented as a reference to compare with the proposed scheme [22]. The decision rule is

$$\hat{a_j} = \begin{cases} 1, & \max\left(z_{d_k,k}\right) \geq \gamma_j, \\ & k \in \mathbb{Z}^+ \text{ and } jN_s \leq k < (j+1)N_s \\ 0, & \text{otherwise.} \end{cases} \tag{43}$$

where $\max\left(z_{d_k,k}\right)$ is the max concentration in the jth interval. γ_j is the threshold. $\hat{a_j}$ is the detected symbol value in the jth interval. With the detected symbol values, their ISI in the current interval is calculated and added on the threshold γ_j to fight the ISI effect in the detection. The initial threshold γ_0 is set as the half of the channel IR peak value of the initial distance d_0. All the calculations in this method are based on the fixed distance (i.e. initial distance) between the transmitter and the receiver.

To quantitatively evaluate the performance of different detection schemes, the BER is used as the performance metric [29]. For N_{tr} transmitted symbols, N_e symbols are incorrectly detected by the receiver. BER is defined as

$$\text{BER} = \frac{N_e}{N_{\text{tr}}}. \tag{44}$$

A lower BER indicates a better performance.

All the simulations are conducted within the lifetime which is defined in Section III. The complete detection algorithm is described in Algorithm 1.

Algorithm 1 The Proposed Adaptive Detection Algorithm

Initialization: set $ISIFlag$ = 0, d_{ave} = 0, $FormerDistance$ = initial distance, $DetectedSignal$ = 0.

for $ii = 1 : B$ **do**

Sample (t_1, C_1), ..., (t_{Ns}, C_{Ns}) in current interval;

if $ISIFlag$!= 0 **then**

Remove ISI of former bits based on $FormerDistance$ and $DetectedSignal$;

end if

Calculate current interval's $d_{\text{ave}}(ii)$ from samples (t_1, C_1), ..., (t_{Ns}, C_{Ns}) by (31);

Reconstruct IR with current $d_{\text{ave}}(ii)$ using (9);

Record amplitude C_{max} and time T_{max} of the peak point of the reconstructed IR;

if CATD detection method is chosen **then**

Utilize criteria of (35) and (43) to perform detection;

end if

if PAD detection method is chosen **then**

Utilize criteria of (37) and (38) to perform detection;

end if

Record the detected signal value in $DetectedSignal(ii)$

if $DetectedSignal(ii)$ == 1 **then**

$FormerDistance$= $d_{\text{ave}}(ii)$

end if

if $DetectedSignal$!= 0 **then**

$ISIFlag$ = 1;

end if

end for

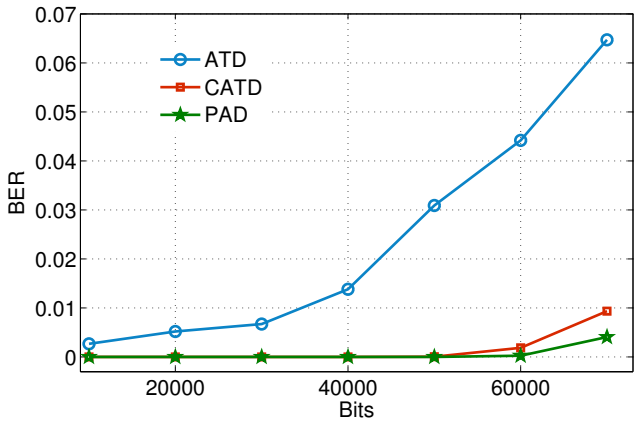

Fig. 11. The impact of symbol sequence length on the BER performance for different detection schemes.

B. Investigation of Symbol Sequence Length

Based on the mobility model, the increase of the released symbol sequence length increases the possibility of a larger distance change with respective to the initial distance d_0. In this subsection, The impact of released symbol sequence length on the performance of detection schemes for mobile MC is evaluated.

The simulation result is shown in Fig. 11. BER here represents the bit error rate of the entire sequence. The symbol sequence length changes from 1×10^4 bits to 7×10^4 bits with a step of 1×10^4 bits. The life time of the system is $d_{\text{end}} = d_0\sqrt{m}$ with $m = T_b/t_{0,\text{peak}}$ as defined at the end of Section III. With parameters in Table II, we have $m = 4$, $d_0 = 12$ μm and $d_{\text{end}} = 24$ μm. We check that the distances in this simulation of the symbol sequence length are all smaller than $d_{\text{end}} = 24$ μm. Therefore, in the simulation, the dynamic distances do not go beyond the lifetime distance d_{end} and the communication link is alive for the results shown. From the result, it is seen that BER increases as the symbol sequence length increases for all of the three detection methods. The proposed CATD and PAD detection methods outperform the ATD method.

For the reference ATD detection, the threshold for the current symbol is calculated as the sum of the initial threshold and the current ISI. In the simulation based on our system model, the averaged distance becomes larger as the symbol sequence increases. Because the reference ATD method considers fixed transmitter and receiver, and therefore fixed distance, so the distance used for estimating ISI is smaller than the actual distance after a number of symbol bits are sent. Then the estimated ISI is bigger than the actual ISI. Therefore, the estimated threshold,

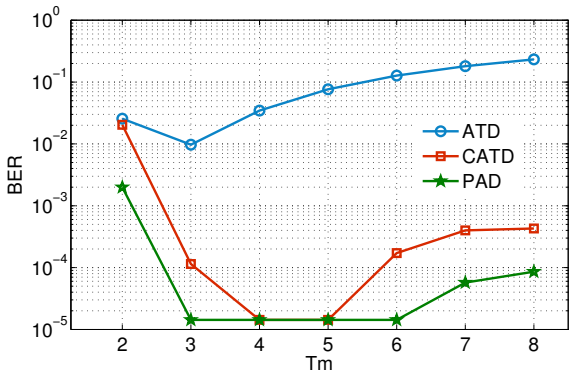

Fig. 12. The impact of symbol interval on the BER performance of different detection schemes for mobile MC.

which is the sum of the initial threshold and the current ISI, becomes bigger than it should be. The error of this threshold calculation leads to wrong detection.

BER of both CATD and PAD methods also increases as the symbol sequence length increases. As the distance from former symbol "1" is utilized for ISI mitigation, error exists in the estimated distance and the reconstructed IR which further affects the signal detection. Furthermore, once there is a symbol "1" decoded incorrectly as "0", the ISI of this symbol "1" in the following symbols cannot be counted and cannot be removed. This leads to more residual molecules in the following sequence and affects the detection. As the released symbol sequence length increases, errors keep accumulating and result in a worse performance.

It can be seen that PAD performs better than CATD, especially when the data sequence length is larger than 5×10^4. The reason is that CATD is more sensitive to distance than PAD. Hence, PAD has a better tolerance to the distance error than CATD. In PAD, the detection is based on the peak time. The peak time value is calculated by (33) and its derivative with respect to distance is shown in (45) which presents its sensitivity to distance. In CATD, the detection is based on peak amplitude. The peak amplitude is obtained in (34). Its derivative with respect to distance is (46) which presents its sensitivity to distance. To compare two methods' sensitivity to distance, we calculate absolute value of (45) and (46). With the parameters in Table II, the absolute value of (46) for CATD is larger than that of (45) for PAD. This indicates that CATD is more sensitive and easily affected by the distance error than PAD.

$$\frac{\mathrm{d}\ t_{j,\text{peak}}}{\mathrm{d}\ d_{j,\text{ave}}} = \frac{d_{j,\text{ave}}}{3D}, \tag{45}$$

$$\frac{\mathrm{d}\ h(t_{j,\text{peak}})}{\mathrm{d}\ d_{j,\text{ave}}} = \frac{-3e^{-\frac{3}{2}}}{(\frac{2\pi}{3})^{(\frac{3}{2})} d_{j,\text{ave}}^4}. \tag{46}$$

C. Investigation of Symbol Interval

Symbol interval is an important parameter in the MC system. It determines the data rate and affects the ISI effect. In this part, the impact of symbol interval on the schemes for the mobile MC is investigated. In the simulation, system parameters in Table II are adopted. We use normalized symbol interval $T_m = \frac{T_b}{t_{0,\text{peak}}}$ instead of T_b. In each run, T_m changes from 2 to 8 with a step of 1. The corresponding T_b value changes from $2 \times t_{0,\text{peak}}$ to $8 \times t_{0,\text{peak}}$ with a step of $t_{0,\text{peak}}$.

Simulation result is shown in Fig. 12. The proposed CATD and PAD perform better than the ATD scheme. For the proposed CATD and PAD methods, the BER firstly decreases, and then gradually increases with respect to T_m. The larger BER at the small values of T_m is due to the severer ISI effect at small symbol interval. As the symbol interval increases, the ISI effect is alleviated and therefore the BER decreases. As the increase of T_m, the BER starts to increase. This is because, with larger symbol interval T_b, the dynamic range of the distance in an interval increases and index $r = \frac{V_r \times T_b}{d_0}$ in (42) increases too. Therefore, d_{ave}^i is not as a good representative of the dynamic range in a large interval as in a small one. The difference between the averaged distance d_{ave}^i and the true distance range in one interval increases. This further causes a larger difference between the reconstructed IR and the true IR. This affects the signal detection accuracy. Meanwhile, the reconstructed IR is also used in the ISI estimation. The inaccuracy of the reconstructed IR leads to the inaccuracy of the ISI calculation and mitigation. Although increasing T_m reduces ISI effect, the result manifests that the impact of increased inaccuracy of the reconstructed IR overwhelms the impact of reduced ISI effect and results in a larger BER. Among the two proposed methods, PAD performs better than the CATD due to that PAD is more robust to the distance estimation error.

D. Investigation of Initial Distance

In this part, the impact of the initial distance d_0 on the performance of detection schemes is investigated. In this simulation, system parameters in Table II are adopted. In each run, d_0 changes from 12 to 36 μm with a step of 3 μm.

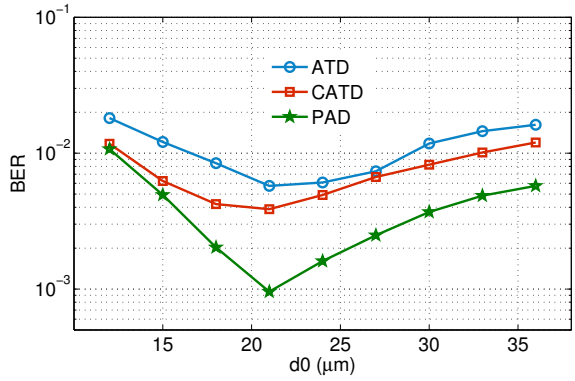

Fig. 13. The impact of initial distance d_0 on the BER performance of different detection schemes for mobile MC.

The simulation result is shown in Fig. 13. Both the proposed CATD and PAD method outperform the ATD method. The BER of all methods decreases as d_0 increases before the initial distance reaches 21 μm. However, after 21 μm, the BER of both detection methods increases as the initial distance d_0 keeps increasing. Two effects explain this phenomenon. The first is that larger initial distance d_0 has a smaller index r in (42) which indicates a smaller relative change of the distance in an interval. Accordingly, the reconstructed IR with d_{ave} is a better representative of the true IR. The signal detection will be more effective. Hence, the detection accuracy increases with the distance. The other impact with the increase of the initial distance d_0 is the shape change of the IR. With larger d_0, the amplitude of IR becomes smaller and the peak time increases, meaning that more molecules will arrive at the receiver outside its own interval and becomes the ISI to the following signals. This increased ISI may be the reason that the BER increases as d_0 increases. These two impacts compete with each other to determine the final BER performance. It is possible that the first impact dominates the performance before 21 μm and the second impact dominates after 21 μm.

Among the two proposed methods, PAD outperforms CATD. Similar to the investigations of symbol sequence length and interval, this is because PAD is more robust to distance error.

E. Investigation of the Number of Released Molecules

As stated in Section III-B, in the OOK MC system, N molecules are released when transmitting symbol "1". The influence of the value of N is investigated. From Fig. 14, it is seen that as the increase of the value of N from 2×10^5 to 12×10^5 with a step of 2×10^5, the BER decreases for all

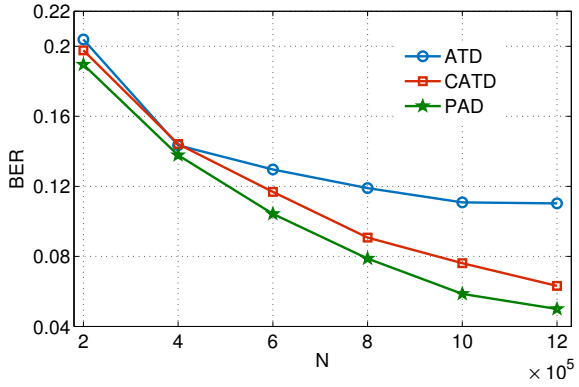

Fig. 14. The impact of the number of released molecules for bit "1" on the BER performance of different detection schemes for the mobile MC.

the three methods. The reason can be explained as following: The noise variance is proportional to the signal amplitude, which is shown in (14). The instantaneous SNR can be simply calculated as $\frac{x^2[d(t),t]}{\sigma_c^2(t)} = V_R \times x[d(t),t]$. Therefore, the larger the signal amplitude is, the larger the SNR is. The signal amplitude is proportional to the number of released molecules, hence, larger N leads to larger SNR. With larger SNR, the distance estimation and IR reconstruction will be more accurate. The ISI mitigation is then more effective. Hence, the accuracy of the signal detection is improved. Similar to the above investigations, PAD and CATD outperform ATD. And PAD is more robust to the inaccuracy of the distance estimation and therefore achieves better performance than CATD.

VII. Conclusion

The existing detection schemes for static MC communication system are not suitable for the mobile MC because of the random varying CIR in mobile MC communication systems. In this paper, we propose two adaptive detection schemes for the mobile MC. A well studied flagellated bacteria, *E. coli*, is considered as a mobile receiver performing random walk. Three-dimensional channel model is established. The adaptive detection scheme includes three main parts which are adaptive ISI mitigation, distance estimation and IR reconstruction, and two adaptive detection methods PAD and CATD. By adaptively using the estimated distance to calculate the ISI and subtract it from the concentration samples, the detection schemes effectively decode original data sequence in the mobile MC system.

The proposed detection schemes are evaluated by Monte Carlo simulations. The simulation results show that the proposed detection schemes outperform the adaptive threshold strategy for the static MC which does not consider the mobility feature. Among the two detection schemes, PAD outperforms CATD because PAD is more robust to the inaccuracy of the distance estimation. The impacts of important system factors including symbol sequence length, symbol interval, initial distance, and number of released molecules are also studied.

In future work, there are two related open issues. Firstly, the data rate in the current system is too low. High data rate scenario detection schemes are expected. Secondly, detection schemes for other modulation methods such as MoSK in mobile MC are expected to be investigated.

REFERENCES

[1] I. F. Akyildiz, J. M. Jornet, and M. Pierobon, "Nanonetworks: A new frontier in communications," *Commun. ACM*, vol. 54, no. 11, pp. 84–89, Nov. 2011.

[2] T. Nakano, M. J. Moore, F. Wei, A. V. Vasilakos, and J. Shuai, "Molecular communication and networking: Opportunities and challenges," *IEEE Trans. Nanobiosci.*, vol. 11, no. 2, pp. 135–148, Jun. 2012.

[3] T. Nakano, T. Suda, Y. Okaie, M. J. Moore, and A. V. Vasilakos, "Molecular communication among biological nanomachines: A layered architecture and research issues," *IEEE Trans. Nanobiosci.*, vol. 13, no. 3, pp. 169–197, Sep. 2014.

[4] R. Gupta, M. Sharma, and A. Mittal, "Effects of membrane tension on nanopropeller driven bacterial motion," *Journal of Nanoscience and Nanotechnology*, vol. 6, no. 12, pp. 3854–3862, 2006.

[5] Y. Okaie, T. Nakano, T. Hara, T. Obuchi, K. Hosoda, Y. Hiraoka, and S. Nishio, "Cooperative Target Tracking by a Mobile Bionanosensor Network," *IEEE Trans. Nanobiosci.*, vol. 13, no. 3, pp. 267–277, Sep. 2014.

[6] N. Farsad, H. B. Yilmaz, A. Eckford, C. B. Chae, and W. Guo, "A comprehensive survey of recent advancements in molecular communication," *IEEE Commun. Surveys Tuts*, vol. 18, no. 3, pp. 1887–1919, Third Quarter 2016.

[7] N.-R. Kim and C.-B. Chae, "Novel modulation techniques using isomers as messenger molecules for nano communication networks via diffusion," *IEEE J. Sel. Areas Commun.*, vol. 31, no. 12, pp. 847–856, Dec. 2013.

[8] L. Lin, C. Yang, J. Wang, and S. Ma, "Evaluation of digital baseband modulation schemes for molecular communication in nanonetworks," in *Proc. IEEE ICUFN*. IEEE, 2014, pp. 297–302.

[9] L.-S. Meng, P.-C. Yeh, K.-C. Chen, and I. F. Akyildiz, "On receiver design for diffusion-based molecular communication," *IEEE Trans. Signal Process.*, vol. 62, no. 22, pp. 6032–6044, Nov. 2014.

[10] D. Kilinc and O. B. Akan, "Receiver design for molecular communication," *IEEE J. Sel. Areas Commun.*, vol. 31, no. 12, pp. 705–714, Dec. 2013.

[11] A. Guney, B. Atakan, and O. B. Akan, "Mobile ad hoc nanonetworks with collision-based molecular communication," *IEEE Trans. Mobile Comput.*, vol. 11, no. 3, pp. 353–366, Mar. 2012.

[12] L. Felicetti, M. Femminella, and G. Reali, "Establishing digital molecular communications in blood vessels," in *Proc. IEEE BlackSeaCom*, 2013, pp. 54–58.

[13] Z. Luo, L. Lin, and M. Ma, "Offset estimation for clock synchronization in mobile molecular communication system," in *Proc. IEEE WCNC*. IEEE, 2016, pp. 1–6.

[14] M. Kuscu and O. B. Akan, "A communication theoretical analysis of fret-based mobile ad hoc molecular nanonetworks," *IEEE Trans. Nanobiosci.*, vol. 13, no. 3, pp. 255–266, Sep. 2014.

[15] ——, "Coverage and throughput analysis for fret-based mobile molecular sensor/actor nanonetworks," *Nano Commun. Netw.*, vol. 5, no. 1, pp. 45–53, May 2014.

[16] S. Qiu, T. Asyhari, and W. Guo, "Mobile molecular communications: Positional-distance codes," in *Proc. IEEE SPAWC*, July 2016, pp. 1–5.

[17] H. C. Berg, *Random walks in biology*. Princeton University Press, 1993.

[18] A. Ahmadzadeh, V. Jamali, A. Noel, and R. Schober, "Diffusive mobile molecular communications over time-variant channels," *IEEE Commun. Lett.*, 2017.

[19] Q. Wu, L. Lin, Z. Luo, and H. Yan, "Bit alignment scheme for mobile receiver in molecular communication," in *Proc. IEEE ICUFN*. IEEE, 2017, pp. 750–752.

[20] I. Llatser, E. Alarcón, and M. Pierobony, "Diffusion-based channel characterization in molecular nanonetworks," in *Proc. IEEE INFOCOM*. IEEE, 2011, pp. 467–472.

[21] B. Li, M. Sun, S. Wang, W. Guo, and C. Zhao, "Low-complexity noncoherent signal detection for nanoscale molecular communications," *IEEE Trans. Nanobiosci.*, vol. 15, no. 1, pp. 3–10, Jan. 2016.

[22] B. Tepekule, A. E. Pusane, H. B. Yilmaz, C.-B. Chae, and T. Tugcu, "ISI mitigation techniques in molecular communication," *IEEE Trans. Mol. Biol. Multi-Scale Commun.*, vol. 1, no. 2, pp. 202–216, Jun. 2015.

[23] M. S. Kuran, H. B. Yilmaz, T. Tugcu, and I. F. Akyildiz, "Modulation techniques for communication via diffusion in nanonetworks," in *Proc. IEEE ICC*. IEEE, 2011, pp. 1–5.

[24] W. Guo, T. Asyhari, N. Farsad, H. B. Yilmaz, B. Li, A. Eckford, and C. B. Chae, "Molecular communications: channel model and physical layer techniques," *IEEE Wireless Commun.*, vol. 23, no. 4, pp. 120–127, Aug. 2016.

[25] M. U. Mahfuz, D. Makrakis, and H. T. Mouftah, "On the characterization of binary concentration-encoded molecular communication in nanonetworks," *Nano Commun. Netw.*, vol. 1, no. 4, pp. 289–300, Dec. 2010.

[26] W.-A. Lin, Y.-C. Lee, P.-C. Yeh, and C.-h. Lee, "Signal detection and ISI cancellation for quantity-based amplitude modulation in diffusion-based molecular communications," in *Proc. IEEE GLOBECOM*. IEEE, 2012, pp. 4362–4367.

[27] M. U. Mahfuz, D. Makrakis, and H. T. Mouftah, "A generalized strength-based signal detection model for concentration-encoded molecular communication," in *Proc. The 8th International Conference on Body Area Networks*. ICST (Institute for Computer Sciences, Social-Informatics and Telecommunications Engineering), 2013, pp. 461–467.

[28] ——, "A comprehensive analysis of strength-based optimum signal detection in concentration-encoded molecular communication with spike transmission," *IEEE Trans. Nanobiosci.*, vol. 14, no. 1, pp. 67–83, Jan. 2015.

[29] A. Aijaz and A.-H. Aghvami, "Error performance of diffusion-based molecular communication using pulse-based modulation," *IEEE Trans. Nanobiosci.*, vol. 14, no. 1, pp. 146–151, Jan. 2015.

[30] H. ShahMohammadian, G. G. Messier, and S. Magierowski, "Optimum receiver for molecule shift keying modulation in diffusion-based molecular communication channels," *Nano Commun. Netw.*, vol. 3, no. 3, pp. 183–195, Sep. 2012.

[31] C. T. Chou, "A markovian approach to the optimal demodulation of diffusion-based molecular communication networks," *IEEE Trans. Commun.*, vol. 63, no. 10, pp. 3728–3743, Oct. 2015.

[32] Y.-K. Lin, W.-A. Lin, C.-H. Lee, and P.-C. Yeh, "Asynchronous threshold-based detection for quantity-type-modulated molecular communication systems," *IEEE Trans. Mol. Biol. Multi-Scale Commun.*, vol. 1, no. 1, pp. 37–49, Mar. 2015.

[33] A. Noel, K. C. Cheung, and R. Schober, "Optimal receiver design for diffusive molecular communication with flow and additive noise," *IEEE Trans. Nanobiosci.*, vol. 13, no. 3, pp. 350–362, Sep. 2014.

[34] B. H. Koo, H. B. Yilmaz, C.-B. Chae, and A. Eckford, "Detection algorithms for molecular MIMO," in *Proc. IEEE ICC*. IEEE, 2015, pp. 1122–1127.

[35] A. Einolghozati, M. Sardari, and F. Fekri, "Design and analysis of wireless communication systems using diffusion-based molecular communication among bacteria," *IEEE Trans. Wireless Commun.*, vol. 12, no. 12, pp. 6096–6105, Oct. 2013.

[36] A. Noel, K. C. Cheung, and R. Schober, "Improving receiver performance of diffusive molecular communication with enzymes," *IEEE Trans. Nanobiosci.*, vol. 13, no. 1, pp. 31–43, 2014.

[37] M. Gregori, I. Llatser, A. Cabellos-Aparicio, and E. Alarcón, "Physical channel characterization for medium-range nanonetworks using flagellated bacteria," *Comput. Netw.*, vol. 55, no. 3, pp. 779–791, Oct. 2011.

[38] M. Pierobon and I. F. Akyildiz, "Diffusion-based noise analysis for molecular communication in nanonetworks," *IEEE Trans. Signal Process.*, vol. 59, no. 6, pp. 2532–2547, Jun. 2011.

[39] B. Li, M. Sun, S. Wang, W. Guo, and C. Zhao, "Local convexity inspired low-complexity noncoherent signal detector for nanoscale molecular communications," *IEEE Trans. Commun.*, vol. 64, no. 5, pp. 2079–2091, Jan. 2016.

[40] A. Singhal, R. K. Mallik, and B. Lall, "Performance analysis of amplitude modulation schemes for diffusion-based molecular communication," *IEEE Trans. Wireless Commun.*, vol. 14, no. 10, pp. 5681–5691, 2015.

[41] M. Pierobon and I. F. Akyildiz, "A physical end-to-end model for molecular communication in nanonetworks," *IEEE J. Sel. Areas Commun.*, vol. 28, no. 4, May. 2010.

[42] K. Srinivas, A. W. Eckford, and R. S. Adve, "Molecular communication in fluid media: The additive inverse gaussian noise channel," *IEEE Trans. Inf. Theory*, vol. 58, no. 7, pp. 4678–4692, Apr. 2012.

[43] L. Lin, C. Yang, M. Ma, and S. Ma, "Diffusion-based clock synchronization for molecular communication under inverse gaussian distribution," *IEEE Sensors J.*, vol. 15, no. 9, pp. 4866–4874, Sep. 2015.

[44] L. Lin, C. Yang, M. Ma, S. Ma, and H. Yan, "A clock synchronization method for molecular nanomachines in bionanosensor networks," *IEEE Sensors J.*, vol. 16, no. 19, pp. 7194–7203, Oct. 2016.

[45] L. Lin, J. Zhang, M. Ma, and H. Yan, "Time synchronization for molecular communication with drift," *IEEE Commun. Lett.*, vol. 21, no. 3, pp. 476–479, Mar. 2017.

[46] B. H. Koo, C. Lee, H. B. Yilmaz, N. Farsad, A. Eckford, and C. B. Chae, "Molecular MIMO: From theory to prototype," *IEEE J. Sel. Areas Commun.*, vol. 34, no. 3, pp. 600–614, Mar. 2016.

[47] M. J. Moore, T. Nakano, A. Enomoto, and T. Suda, "Measuring distance from single spike feedback signals in molecular communication," *IEEE Trans. Signal Process.*, vol. 60, no. 7, pp. 3576–3587, Jul. 2012.

[48] A. Noel, K. C. Cheung, and R. Schober, "Bounds on distance estimation via diffusive molecular communication," in *Proc. IEEE GLOBECOM*. IEEE, 2014, pp. 2813–2819.

[49] J.-T. Huang, H.-Y. Lai, Y.-C. Lee, C.-H. Lee, and P.-C. Yeh, "Distance estimation in concentration-based molecular communications," in *Proc. IEEE GLOBECOM*. IEEE, 2013, pp. 2587–2591.

[50] X. Wang, M. D. Higgins, and M. S. Leeson, "Distance estimation schemes for diffusion based molecular communication systems," *IEEE Commun. Lett.*, vol. 19, no. 3, pp. 399–402, 2015.

[51] M. Gregori and I. F. Akyildiz, "A new nanonetwork architecture using flagellated bacteria and catalytic nanomotors," *IEEE J. Sel. Areas Commun.*, vol. 28, no. 4, pp. 612–619, May 2010.